Supplementary Materials for

Determination of the melanocortin-4 receptor structure identifies Ca^{2+} as a cofactor for ligand binding

Jing Yu, Luis E. Gimenez, Ciria C. Hernandez, Yiran Wu, Ariel H. Wein, Gye Won Han, Kyle McClary, Sanraj R. Mittal, Kylie Burdsall, Benjamin Stauch, Lijie Wu, Sophia N. Stevens, Alys Peisley, Savannah Y. Williams, Valerie Chen, Glenn L. Millhauser, Suwen Zhao, Roger D. Cone*, Raymond C. Stevens*

*Corresponding author. Email: rcone@umich.edu (R.D.C.); stevens@shanghaitech.edu.cn (R.C.S.)

Published 24 April 2020, *Science* **368**, 428 (2020)
DOI: 10.1126/science.aaz8995

This PDF file includes:

Other Supplementary Material for this manuscript includes the following:
(available at science.sciencemag.org/content/368/6489/428/suppl/DC1)

Materials and Methods:

Molecular biology

The sequence of the human MC4R gene (UniProt id P32245) was codon-optimized and synthesized by GenScript and was subcloned into a modified pFastBac1 vector containing a haemagglutinin (HA) signal sequence followed by a FLAG tag at the N-terminus, as well as a PreScission protease site, and a 10× His tag at the C-terminus for expression. The modifications, including 15 amino acids truncated at the N-terminus, 12 amino acids truncated at the C-terminus, and PGS fusion protein insertion, were introduced by standard PCR. The biochemical and pharmacological characterization constructs were designed based on the modified pFastBac1 template into pcDNA3.1 vector. The final pcDNA 3.1 vectors contained the same tags as the modified pFastBac1 vector and were modified by introducing 5 mutations (Fig. 2A, C2), plus truncating 15 amino acids at N-terminus (Fig. 2A, C3), truncating 12 amino acids at C-terminus (Fig. 2A, C4), and replacing ICL3 (at residues H222-R236) with a fragment of PGS (residues 218-413) (Fig. 2A, C5).

MC4R expression and purification

The receptor in the modified pFastBac1 vector was expressed in *Spodoptera frugiperda* (*Sf*9) cells using the Bac-to-Bac Baculovirus Expression System (Invitrogen). The recombinant bacmids (2-5 μg) were transfected into *Sf*9 cells to produce recombinant baculovirus. *Sf*9 cells were infected by recombinant baculovirus at a density of 2×10^6 cells per mL with a multiplicity of infection (MOI) of 5 and grown for 48 h at 27°C. Then the cells were harvested by centrifugation and stored at -80°C for future use. Cell membranes were prepared as lysed frozen cell pellets in a hypotonic buffer with 10 mM HEPES (pH 7.0), 10 mM $MgCl_2$, 20 mM KCl, and EDTA-free complete protease inhibitor cocktail tablets (Roche). The membrane fraction was collected by centrifugation at 60,000 g for 30 min. This procedure was repeated twice using the same hypotonic buffer and another three times using hypertonic buffer with 1M NaCl. The purified membrane was flash frozen using liquid nitrogen and stored at -80°C for future use.

Cell membranes were thawed at 4°C and incubated with both EDTA-free complete protease inhibitor cocktail tablets (Roche) and 50 μM SHU9119 (GenScript, Shanghai, China) for 30 min. Afterwards, membranes were incubated in the presence of 2 mg per mL iodoacetamide for 30 min. The MC4R was extracted from membranes in a final buffer comprised of 50 mM HEPES (pH 7.0), 800 mM NaCl, 1.0% (w/v) n-dodecyl-β-D-maltopyranoside (DDM; Anatrace), and 0.2% (w/v) cholesteryl hemisuccinate (CHS; Sigma) and incubated for 3 h at 4°C. The supernatants were collected by centrifugation at 60,000 × g for 30 min and incubated with TALON IMAC resin (Clontech) and 30 mM imidazole overnight at 4°C. The resin was washed with 10 column volumes of wash buffer 1 containing 50 mM HEPES (pH 7.0), 800 mM NaCl, 10% glycerol, 10 mM $MgCl_2$, 0.05% DDM, 0.01% CHS, 30 mM imidazole, 8 mM ATP, and 50 μM SHU9119. Afterwards, the resin was further washed with 20 column volumes of wash buffer 2 containing 50 mM HEPES (pH 7.0), 800 mM NaCl, 10% Glycerol, 0.05% DDM, 0.01% CHS, 30 mM imidazole, and 50 μM SHU9119. At the final step, the protein was eluted in elution buffer containing 50 mM HEPES (pH 7.0), 800 mM NaCl, 10% Glycerol, 0.01% DDM, 0.002% CHS, 220 mM imidazole, and 100 μM SHU9119. The purified protein was incubated with EndoH (in-house production) overnight at 4°C to remove glycosylation. The protein was concentrated to 35-45 mg per mL for crystallization trials using a 100 kDa cutoff concentrator (Sartorius).

Lipidic cubic phase crystallization

The purified MC4R-PGS-SHU9119 complex was reconstituted into lipidic cubic phase (LCP) by mixing with molten lipid containing 90% monoolein and 10% (v/v) cholesterol at a protein/lipid ratio of 2:3 (v/v). The crystallization trials were performed using an automated crystallization robot (NT8, Formulatrix) by overlaying 50 nL mesophase with 800 nL precipitant solution on 96-well glass sandwich plates following incubation at 20°C in an automatic incubator/imager (RockImager 1000, Formulatrix). The crystals grew from buffers containing 19~26% PEG 400, 100 mM Bis-tris propane buffer (pH 7.9~8.1), and 50-100 mM $CaCl_2$•$2H_2O$, and took 6-7 days to reach final size (60-70 µm length). The crystals were harvested using 30-100 µm micromounts (MiTeGen) and were immediately flash frozen in liquid nitrogen.

Data collection and structure determination

Crystal data collection was conducted at the SPring-8 beamline 45XU (Hyogo, Japan). X-ray diffractions were collected using a 10×11 μm^2 (width × height) micro-focused beam (X-ray wavelength 1.0000 Å) and a Pilatus 6M detector. An automatic data collection system (ZOO) developed at SPring-8 was used for data collection (*38*). This included 0.1° rotation, 0.1 s exposure time and 10° rotation per crystal in total. Images were collected following an automatic raster scanning with SHIKA and KAMO automatically processed collected images. Data sets from 84 best-diffracting crystals were integrated and scaled to an overall 2.75 Å resolution using XDS (*39*). Initial phase information of the MC4R-SHU9119 complex was obtained by molecular replacement using the receptor portion of human A_{2A} adenosine receptor (PDB ID 3EML) and the PGS in the CB1 structure (PDB ID 5U09) independently with the program Phaser (*40*). All refinements were performed with Phenix (*41*) and Buster (*42*) followed by manual examination and rebuilding of the refined coordinates in the program Coot (*43*) using both |2Fo|-|Fc| and |Fo|-|Fc| maps. The Ramachandran plot analysis indicated that 100% of the residues were in favorable (97.8%) or allowed (2.2%) regions (no outliers). Data collection and refinement statistics are listed in Table S1.

Fluorescence-based thermal stability assay

Each sample containing approximately 1 µg of purified MC4R with different ligands such as SHU9119, NDP-MSH, α-MSH, AgRP was incubated with different ions including $CaCl_2$, $MgCl_2$ and $ZnSO_4$ (StockOptions™ Salt, Hampton Research, Aliso Viejo CA) for 1 h at 4°C. The samples that were purified with SHU9119 or NDP-MSH were further incubated with 200 µM EDTA (Ethylenediamine tetraacetic acid, Sigma). Afterwards, 1 µL of thiol-N-[4-(7-diethylamino-4-methyl-3-coumarinyl)phenyl]maleimide (CPM) dye (4 mg/mL stock in DMSO) diluted in 25 mM HEPES (pH 7.0), 500 mM NaCl, 0.05% DDM, 0.001% CHS, and 2% glycerol was added at room temperature for 15 min. Temperature curves were measured in a Rotor-Gene Q real-time PCR cycler (QIAGEN, Hilden, Germany) in excitation and detection wavelengths of 345-385 nm and 440-480 nm, respectively. Temperatures ranged from 25-99°C with a step of 1°C per min. Data were fit to a Boltzmann sigmoidal curve to determine T_m values in GraphPad Prism 8.0 (GraphPad Software, San Diego, CA).

Inductively coupled plasma atomic emission spectroscopy (ICP-AES) for element detection

Imidazole was removed from the purified MC4R-SHU9119 protein complex by eluting the sample from a PD MiniTrap G-25 column (GE healthcare) with buffer containing 50 mM HEPES (pH 7.0), 50 mM NaCl, 0.005% DDM, and 0.0001% CHS. Then the protein was concentrated to

5.25 mg/mL using a 100 kDa cutoff concentrator (Sartorius). The sample was finally loaded into an Optima™ 8000 ICP optical emission spectrometer (PerkinElmer, Waltham, MA) for element detection including calcium, magnesium and zinc.

Determination of intracellular cAMP levels in live cells

We adopted a genetically encoded split-firefly luciferase reporter that incorporated the cAMP-binding domain B from protein kinase A regulatory subunit type IIβ (RIIβB) at the luciferase hinge region. We next acquired a HEK293 clonal cell line (Promega, Madison, WI) expressing a cAMP-luciferase reporter (GScAMP22f) variant under hygromycin B selection. These cells enabled the measurement of rapid kinetic intracellular cAMP luminescence responses from G_s-coupled receptor activation. Since MC4R couples to G_s, this assay provided a sensitive and specific platform to assess the coupling to G_s of the different MC4R crystallization construct derivatives (Fig. 2A) used in this study.

To determine the effect of the different modifications required to generate the crystallization construct (C5) on Gs coupling and adenylyl cyclase activation, we transfected constructs C1 through C5 (Fig. 2A) as well as mutant D122$^{3.25}$A. Prior to transfections, cells were grown and maintained in selection media consisting of Dulbecco's modified Eagle media (DMEM) with 4.5 g/L D-glucose, and 4 mM L-glutamine (Thermo Fisher Scientific, Waltham, MA), supplemented with 10% fetal bovine serum, 100 units/mL penicillin, 100 µg/mL streptomycin, 2.5 µg/mL amphotericin B, and 200 µg/mL hygromycin B for positive selection of the GScAMP22f reporter. A day before transfection, cells were seeded onto 100 mm cell culture dishes at a density of 6×10^6 cells/dish. Plasmids were transfected (10 µg per dish) using Lipofectamine 3000 (Thermo Fisher Scientific) following the protocol suggested by the manufacturer. A day before readings were performed (24 h after transfection), cells were dissociated, the suspension was adjusted to 1×10^6 cells/mL, and 20 µL were added to individual wells of 384-well poly-D lysine-coated, clear bottom, and black-wall cell culture plates (Corning Inc. Corning, NJ). Plated cells were incubated for an additional 18 to 24 h inside a humidified incubator under 5% CO_2 atmosphere at 37°C.

On the day assays were performed, cell culture media was removed from the plates by a quick hand flick and gentle blotting on absorbent paper. A 4% D-luciferin (Promega) solution in CO_2 independent medium (Thermo Fisher Scientific) was added to each well and left to equilibrate at 37°C for 2 h when cells were ready to be assayed. Luminescence resulting from intracellular cAMP level changes were measured using an FDSS 7000EX functional drug screening system (Hamamatsu Photonics, Hamamatsu, Japan). This instrument allowed for the *in-line* addition of antagonist compounds (i.e. SHU9119, Tocris Bioscience, Bristol, UK, or $AgRP_{(83-132)}$, expressed, folded and purified in house by V.C. and G.L.M.) and/or receptor agonist while simultaneously acquiring the luminescence signal from live cells. Assay read steps were set as follows: baseline acquisition of 5 min, addition of 10 µL antagonist or vehicle followed by 5 min measurement, and 10 µL addition of various concentrations (depending on assay type) of α-MSH peptide (Bachem, Bubendorf, Switzerland) followed by 10 min response measurement. Baseline luminescence (i.e. the average luminescence signal from the initial 0 to 5 min window) was subtracted from the maximum luminescence obtained during the agonist add window (10 to 20 min) to yield the agonist elicited response in the presence of antagonists or vehicle. EC_{50} or IC_{50} potency values were determined by non-linear regression by fitting the data to a sigmoid variable slope model using the GraphPad Prism version 8.2 software package (San Diego, CA).

Ca^{2+} effect on cAMP signaling

We used the LANCE® Ultra cAMP kit (PerkinElmer) to characterize the effect of Ca^{2+} on α-MSH (or forskolin) concentration-response curves (Figs. 4E and F, respectively) for cAMP levels. HEK293 cells were maintained and transfected (or untransfected when using forskolin) with the MC4R C1 construct (Fig. 2A) as described for the Glo sensor live cell cAMP assay. Forty-eight hours after transfection (when applicable), cells were dissociated and washed twice with Hank's balanced salt solution without calcium or magnesium (Thermo Fisher Scientific). The final pellet was resuspended in Ca^{2+}-free stimulation buffer consisting of 135 mM NaCl, 5 mM KCl, 1 mM EGTA, 5 mM D-glucose, 50 µM 3-Isobutyl-1-methylxanthine (IBMX), and 0.1% BSA in 10 mM HEPES; pH = 7.4 (NaOH) and ~290 mOsmol/kg in the condition devoid of Ca^{2+} ($[Ca^{2+}]$ ~3 nM) or with additional 1.5 mM $CaCl_2$ ($[Ca^{2+}]$ ~0.5 mM). Cell density was adjusted to 1×10^6 cells/mL. A total of 10,000 cells were added to each well of a half-area white opaque 96-well plate (Corning), and stimulated with various concentrations of α-MSH (MC4R C1 transfected cells) or forskolin (untransfected cells). Cells were incubated with ligand for 30 min at room temperature. The rest of the assay was performed following the manufacturer's instructions. Time-resolved FRET signal (665 nm) was measured using a PerkinElmer EnVision® multimode plate reader. The resulting data was fitted to a four-parameters variable slope sigmoid using GraphPad Prism 8.2.

Radioligand binding assays:

To assess the effect of different cations (Fig. 4) on ligand binding, crude cell membrane extracts were prepared from a clone stably expressing the human wild-type MC4R devoid of tags or other exogenous sequences. Alternatively, for the pharmacological characterization of the modifications leading to the crystallization construct or for assessing the effect of Ca^{2+} on α-MSH binding (Figs. S4A, B), transfections were performed as described above for constructs C1 and C5 and crude membrane extracts were prepared 48 h-post transfection. Membrane extracts were prepared by dissociating cells in culture with TrypLE Express (1×) recombinant trypsin (Thermo Fisher Scientific), harvesting by centrifugation at 200 × g, and resuspension in standard phosphate-buffered saline. This cell suspension was washed twice with PBS with 5 min centrifugations at 1,000 × g. The pellet from the initial washes was resuspended in a cold membrane preparation buffer consisting of 50 mM Tris (pH = 7.4) and cOmplete™ EDTA-free protease inhibitor cocktail tablets (Roche). The cell suspension was homogenized using a T10 Ultra Turrax® (IKA Works, Wilmington, NC) homogenizer and the homogenate was centrifuged at 35,000 × g for 20 min. This procedure was repeated twice. The final pellet was weighed and resuspended in 10 × volume of membrane preparation buffer supplemented with 10% sucrose. Membrane extracts were aliquoted and stored at -80°C until used. Total protein content was determined by the bicinchoninic acid assay using the Pierce™ BCA Protein Assay Kit (Thermo Fisher Scientific).

Equilibrium saturation experiments were carried out by incubating varying concentrations of [^{125}I][Nle^4,DPhe^7]-α-MSH (PerkinElmer, Waltham, MA) with 4 µg of total protein from the respective membrane extract in a final volume of 200 µL of assay buffer (25 mM HEPES pH = 7.4, 0.2% BSA). Membranes and radioligand were incubated for 120 min at 25°C, and the bound ligand was separated from the free ligand by rapid filtration through GF/B glass fiber filters (Brandel, Gaithersburg, MD) using a 48-probe cell harvester (Brandel). The filters were transferred to scintillation vials and a scintillation cocktail (Ultima Gold™, PerkinElmer) was added and allowed to embed the filters for 16 to 18 h before counting on a liquid scintillation counter (LS6500, Beckman-Coulter, Brea, CA).

To characterize the effect of different cations on receptor ligand binding (Fig. 4C), a near-to-K_D concentration (80 pM) of ^{125}I-NDP-MSH was assayed in the presence of varying concentrations of $CaCl_2$, $ZnSO_4$, $MgCl_2$, LiCl, or KCl (StockOptions™ Salt, Hampton Research). The different salts were pre-incubated with the membrane extract from a stable cell line expressing the wild-type human MC4R for 30 min at room temperature before addition of the radioligand. The reaction was incubated for an additional 120 min at 25°C.

Competition binding experiments were performed by incubating varying concentrations of different unlabeled melanocortin ligands for 30 min, followed by the addition of radioligand at a close-to-K_D (80 or 150 pM for wild-type or crystallization constructs, respectively) concentration. Experiments were incubated for an additional 120 min at 25°C.

For all experiments, specific binding was determined by subtracting the non-specific binding obtained in the presence of 10 μM NDP-MSH. Binding parameters were determined by fitting a variable-slope isotherm or a variable slope four-parameter sigmoid to the respective dataset using GraphPad Prism 8.2 (GraphPad Software, San Diego, CA).

Cell-surface ELISA:

Plasmids corresponding to C1 through C5, or pcDNA3.1(+) (Invitrogen) empty plasmid were transfected as described above. One day after transfection, cells were re-seeded onto poly-D-lysine treated 24-well plates at a density of 3.5×10^5 cells per well. Forty-eight hours after transfection, cells were washed with Tris-buffered saline (TBS) and fixed with 4% formaldehyde on ice for 15 min followed by three washes with TBS. Following fixation, cells were blocked with blocking buffer (1% BSA in TBS) for 2 h at room temperature. Afterwards, plates were incubated with a 1:2,500 dilution of anti-FLAG M2 HRP-conjugated monoclonal antibody (Millipore Sigma Cat# A8592) in blocking buffer for two additional hours at room temperature with gentle agitation. After careful washing, 200 μL per well of 3,3',5,5'-Tetramethylbenzidine (TMB) peroxidase substrate (Thermo Fisher Scientific) was added. The chromogenic reaction was stopped after 3 min by transferring 100 μL of the TMB supernatant to a clear 96-well plate that was preloaded with 100 μL of 1 M H_2SO_4. Absorbance of the chromogenic reaction was measured at 450 nm. In order to account for variations in cell number, the remaining fixed cells were carefully washed and stained with Janus green B (Sigma-Aldrich). After eluting the stain with 0.5 N HCl and transferring the stained solution to a 96-well clear plate, absorbance was measured at 595 nm. This result is proportional to the cell number plated onto the initial 24-well plates and was used to normalize the absorbance from the HRP-oxidized TMB. Results were expressed as the ratio between absorbance at 450 nm and 595 nm.

Electrophysiology:

For cellular recordings, HEK293T cells (ATCC) were cultured at 37°C in a humidified 5% CO_2 incubator and maintained in Dulbecco's modified Eagle's medium (Invitrogen) supplemented with 10% fetal bovine serum (Atlanta Biologicals, Flowery Branch, GA), and 1% antibiotic-antimycotic (Thermo Fisher Scientific). Cells were plated on 12 mm coverslips (Carolina Biological Supply, Burlington, NC) and transfected after 24 h with X-tremeGENE HP DNA Transfection Reagent (Roche Diagnostics) following the manufacturer's protocol. Whole cell voltage-clamp recordings were performed at room temperature 36-48 h after transfection with Kir7.1-M125R channels and MC4R-C1 and C5 (Fig. 2A) or the MC4R-D122$^{3.25}$N mutant. Cells were bathed in an external solution containing 135 mM NaCl, 2 mM $CaCl_2$, 5 mM KCl, 1 mM $MgCl_2$, 5 mM glucose, and 10 mM HEPES (pH 7.4, ~290 mOsM). Recording electrodes were

pulled from thin-walled borosilicate capillary glass (World Precision Instruments, Sarasota, FL) using a P2000 laser electrode puller (Sutter Instruments, Novato, CA), fire-polished with a Microforge (Narishige, Tokyo, Japan), and filled with an internal solution containing 140 mM KCl, 5 mM $MgCl_2$, 10 mM HEPES, 1 mM EGTA, and 5 mM Na^{2+}-ATP (pH 7.4, ~275 mOsM). All patch electrodes had a resistance of 2 – 4 MΩ. Cells were placed in a 500-µL perfusion chamber through which solution flowed at 4 mL/30 s. Inflow to the chamber was by gravity from several reservoirs, selectable by activation of solenoid valves (Warner Instruments, Hamden, CT). Bath solution exchange was essentially complete in <4 s. Cells were voltage-clamped at -60 mV using an Axopatch 200B amplifier (Axon Instruments, San Jose, CA). To evaluate the effects of
MC4R on channel response, we measured the current amplitudes at -180 mV during application of various concentrations of α-MSH or AgRP followed by 30 mM $BaCl_2$ to determine by elimination, the Ba^{2+}-sensitive Kir7.1 currents. All currents were low-pass filtered at 2 kHz, digitized at 5-10 kHz, and analyzed using the pCLAMP 10 software suite (Molecular Devices). IC_{50} and EC_{50} values were determined by fitting a variable-slope, four parameters, sigmoid model
to concentration-response curves using constrained nonlinear regression analyses performed with GraphPad Prism version 8.2. Concentration-response curves for α-MSH in the presence or absence of 0.5 mM Ca^{2+} (Fig. 4G) were obtained by replacing the standard external bath solution with the Ca^{2+}-free buffer described for the cAMP accumulation assays supplemented with 1.5 mM $CaCl_2$ accordingly.

Figure S1

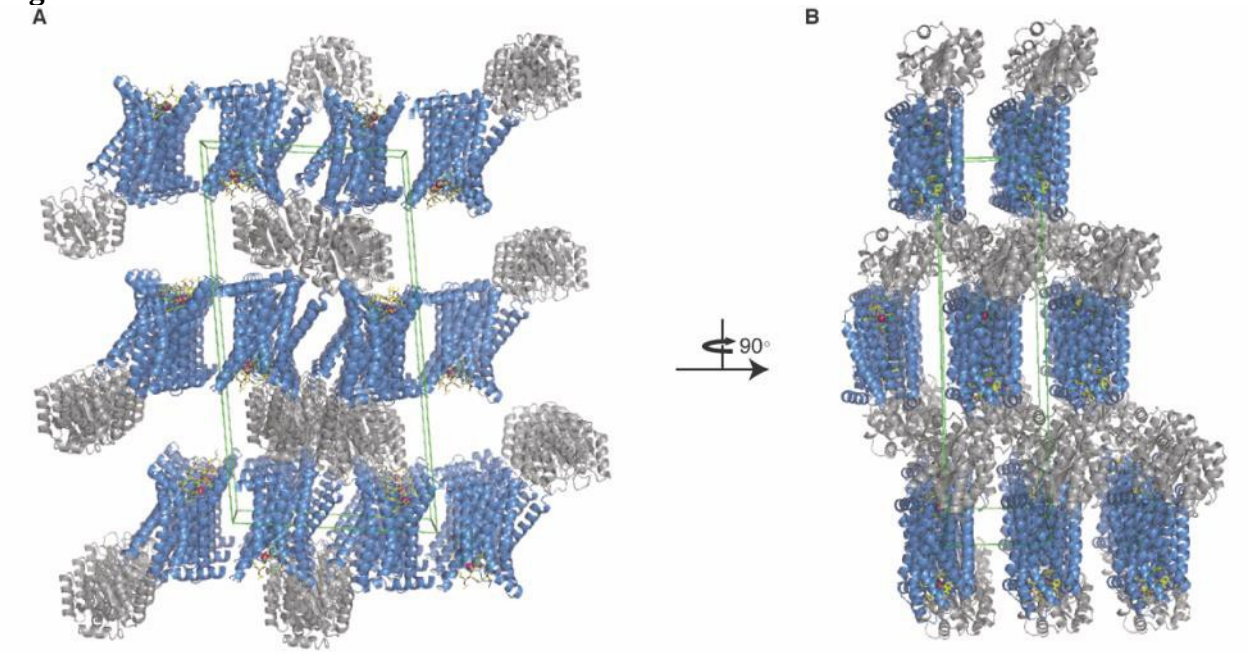

Fig. S1. Crystal packing of the MC4R-SHU9119 complex. (A, B) The unit cell is delimited by the 3D green box. MC4R, SHU9119, and metal ion are shown as blue ribbons, yellow sticks, and a pink sphere, respectively. The PGS fusion is depicted as gray ribbons.

Figure S2

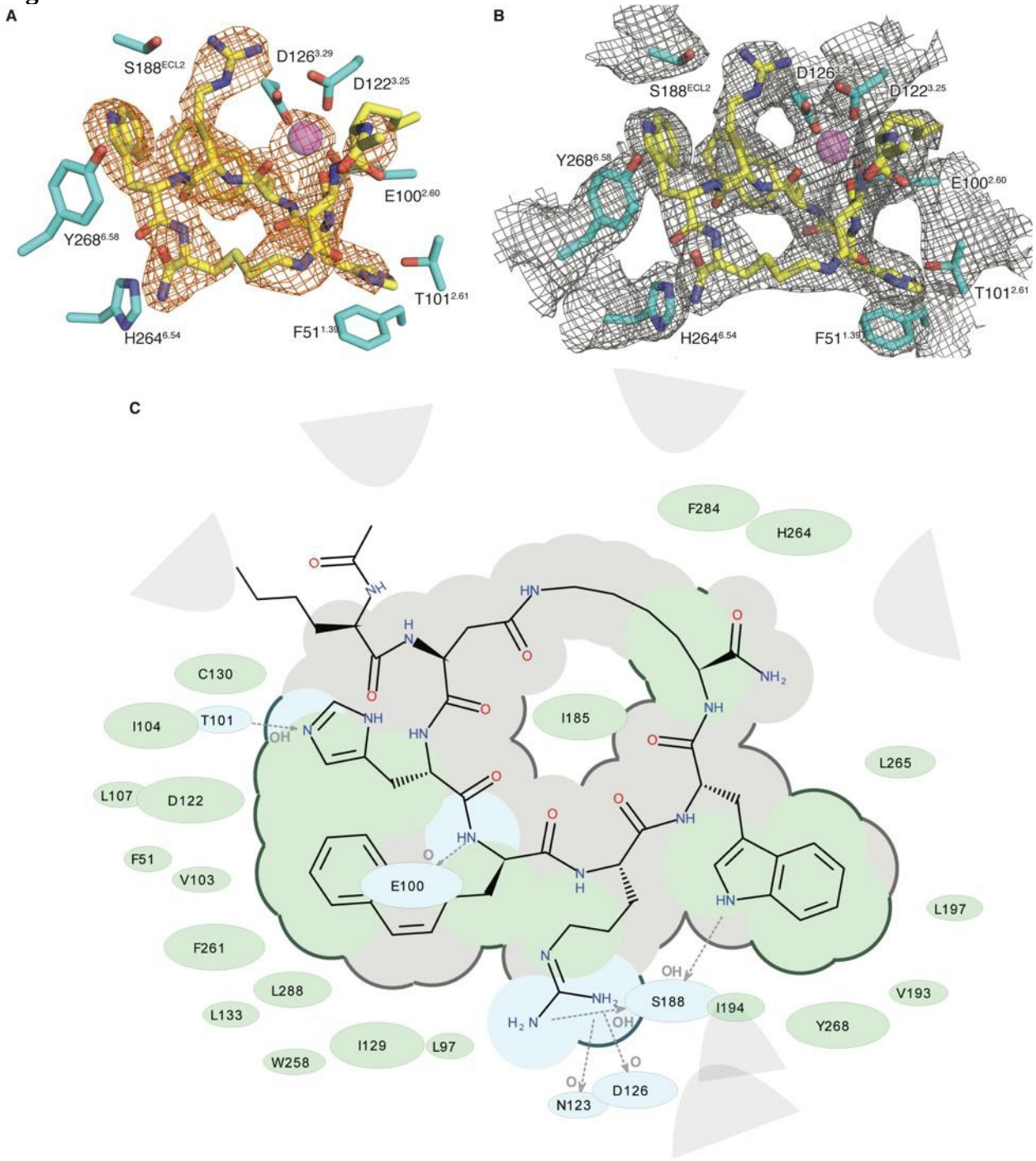

Fig. S2. The MC4R-SHU9119 binding pocket. (A) |Fo|-|Fc| omit maps of SHU9119 and the metal ion are shown as orange mesh. The SHU9119 backbone is shown as yellow sticks and metal ion as pink sphere. Electron densities are contoured at 2.5 σ. **(B)** |2Fo|-|Fc| map of the ligand binding pocket. Electron-densities are shown as gray mesh contoured at 1.0 σ. **(C)** Interactions between SHU9119 and MC4R shown in 2D rendered in ICM-Pro Version 3.8-5 (MolSoft LLC, San Diego, CA). Hydrophobic regions and hydrogen bond acceptors are shown in green and blue shading, respectively. Grey dashed arrows represent hydrogen bonds and grey parabolas represent

broader accessible surface areas. The broken thick line around the ligand indicates accessible surfaces. The size of the colored ellipse around the residues represents the contact strength. 2D-distance between a given residue label and the ligand is indicative of proximity. The binding pocket is cut at a distance of 4.5 Å for the ligand interaction from the surface of the extracellular projection view (except Nle_1 residue of SHU9119 for clarity).

Figure S3

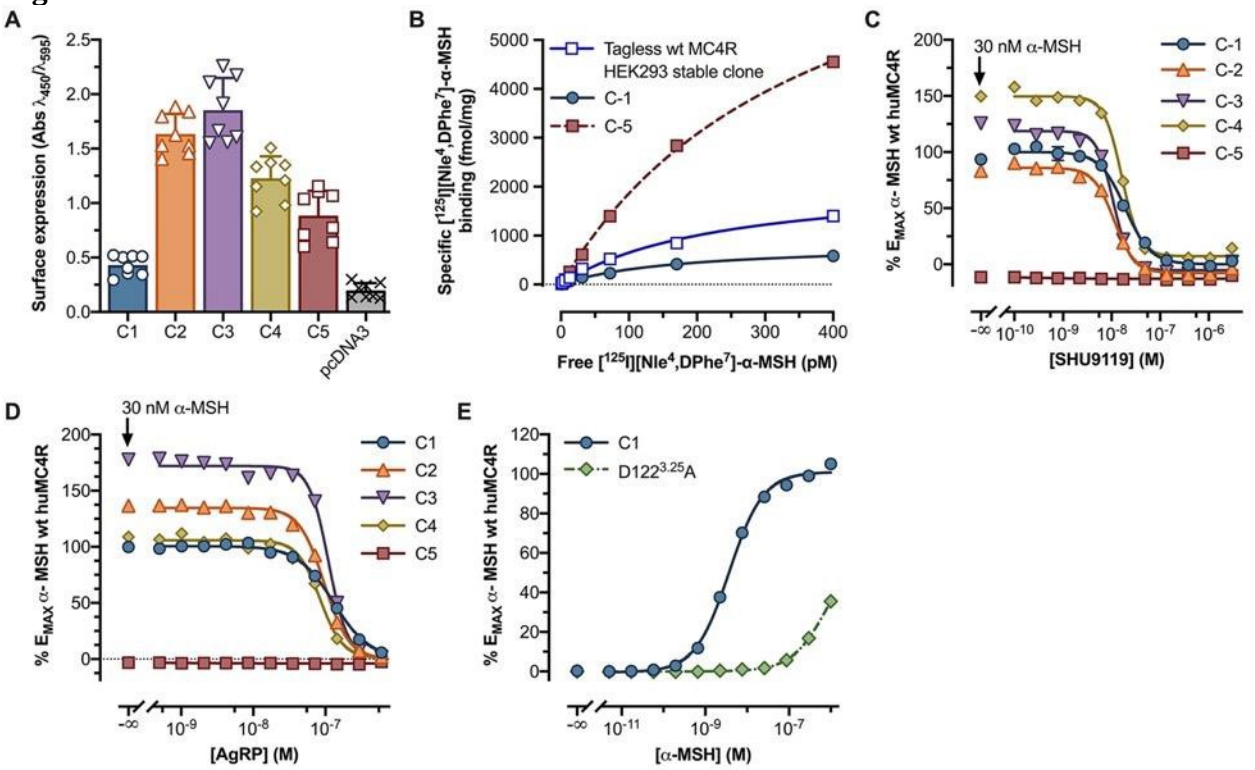

Fig. S3. Surface expression and pharmacological characterization of MC4R constructs with thermostabilizing mutations, N- and C- termini deletions, and PGS fusion. (A) Relative cell surface expression of indicated constructs after transient transfection in HEK293 cells. Bars represent the mean ± standard error of the ratio of peak absorbance (450 nm) for 3,3',5,5'-tetramethylbenzidine (TMB) oxidation over peak absorbance (595 nm) for Janus green B oxidation. **(B)** Saturation binding of [^{125}I][Nle^{4},DPhe^{7}]-α-MSH to membrane extracts from HEK293 cells transfected with constructs C1, C5, or membranes from a stable HEK293 clone expressing untagged wild-type human MC4R. **(C)** Live-cell SHU9119 and **(D)** AgRP$_{(83-132)}$ inhibition in the presence of an EC$_{90}$-equivalent (30 nM) α-MSH concentration for cAMP accumulation. This was measured as luminescence response using a cAMP split-luciferase reporter stably expressed in HEK293 cells transiently transfected with constructs C1 – C5. **(E)** Live-cell α-MSH concentration response curves for cAMP production measured as luminescence response as shown in Fig. 2C with construct C1, and the MC4R D122$^{3.25}$A mutant.

Figure S4

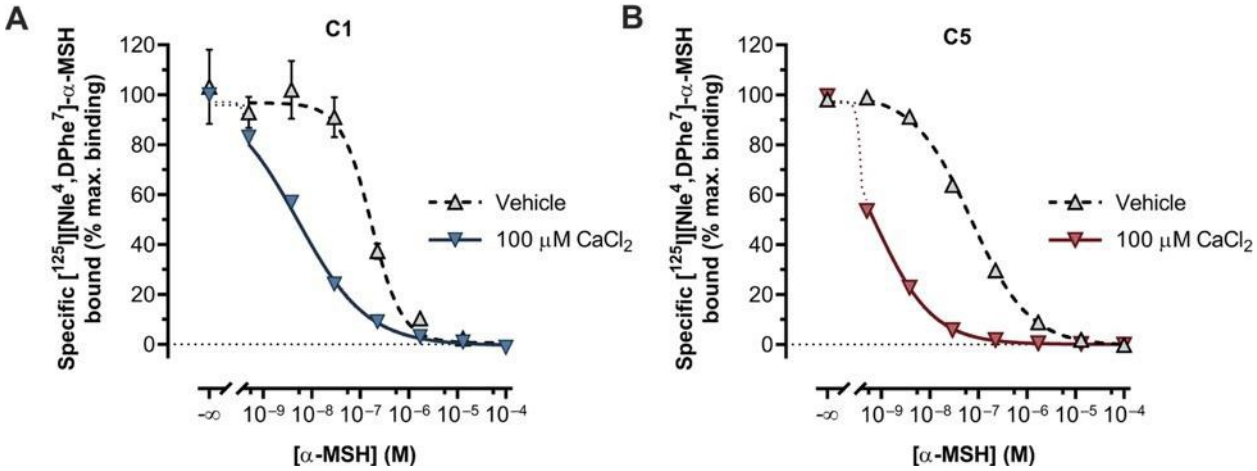

Fig. S4. Effect of Ca^{2+} on the binding affinity of α-MSH for the tagged wild-type MC4R (C1) and thermostabilizing mutations, N- and C- termini deletions, and PGS fusion constructs (C5). (A and B) Competition binding experiments for α-MSH and 80 pM ^{125}I-NDP-MSH to membrane extracts from HEK293 cells transfected with constructs C1 (panel A) or C5 (panel B). Data points represent the mean ± standard error from a representative experiment of two independent experiments with 6 replicates each.

TABLE S1

Data collection and refinement statistics (molecular replacement)

	MC4R- SHU9119
Data collection	
No. of crystals	84
Space group	C 1 2 1
Cell dimensions	
a, *b*, *c* (Å)	163.91, 44.49, 88.05
α, β, γ (°)	90.00, 97.47, 90.00
Resolution (Å)	43.65-2.75 (2.80-2.75)[1]
R_{merge}	0.234 (3.302)
$I / \sigma I$	11.62 (0.96)
$CC_{1/2}$	0.997 (0.561)
Completeness (%)	100 (100)
Redundancy	15.0 (14.5)
Refinement	
Resolution (Å)	43.65-2.75
No. reflections	16,759
R_{work} / R_{free}	0.233 / 0.259
No. atoms	
Protein	3,628
Ligand/ion	78 / 1
Lipids and waters	114
B-factors (Å^2)	
Protein	79.8
Ligand/ion	74.5 / 84.9
Lipids and waters	86.8
RMSD	
Bond lengths (Å)	0.008
Bond angles (°)	0.98

[1]Values in parentheses are for highest-resolution shell.

TABLE S2

Comparison of root-mean squared deviation (RMSD) value between the MC4R structure and other reported GPCR structures

	Receptor Name	Abbreviation	PDB ID (ref)	RMSD[1] (TM Cα, Å)
Lipidic receptors	Lysophosphatidic acid receptor 1	$LPAR_1$	4Z35 (*44*)	2.251
	Cannabinoid receptor 1	CB_1R	5TGZ (*45*)	2.272
	Sphingosine 1-phosphate receptor 1	S1P1R	3V2Y (*46*)	2.371
	Cannabinoid receptor 2	CB_2R	5ZTY (*47*)	2.566
	Thromboxane A2 receptor	TPR	6IIU (*48*)	2.583
Peptidic receptors	Orexin type 1 receptor	OX_1R	4ZJ8 (*49*)	2.466
	Neurotensin type 1 receptor	NTS_1R	4BUO (*50*)	2.518
	C5a anaphylatoxin chemotactic receptor 1	$C5A_1R$	5O9H (*51*)	2.541
	Neurokinin 1 receptor	NK_1R	6HLO (*52*)	2.555
	Orexin type 2 receptor	OX_2R	5WQC (*53*)	2.564

[1] The RMSD values of Cα atoms in transmembrane helices were calculated using UCSF Chimera version 1.13 for edge attribute. In total 192 residues were included: Ballesteros-Weinstein numbers 1.35-1.57, 2.37-2.63, 3.22-3.56, 4.39-4.63, 5.36-5.65, 6.33-6.59, 7.31-7.55.

TABLE S3

^{125}I-NDP-MSH affinity and receptor density for wild-type and crystallization constructs C1 and C5

Construct or cell type	K_D (pM)[1]	B_{MAX} (fmol/mg)[1]
Tag-less wild-type human MC4R HEK293 stable cell clone	235 ± 43	2,179 ± 196
C1: Wild-type Flag-huMC4R-10xHis	170 ± 22	830 ± 48
C5: Flag-huMC4R-10xHis (E49$^{1.37}$V, N97$^{2.57}$L, S99$^{2.59}$F, S131$^{3.34}$A, D298$^{7.49}$N) + ΔN-Term^{M1-L15} + ΔC-Term$^{P321-Y332}$ + *Pyrococcus abyssi* glycogen synthase fragment fusion from residues H222-R236	377 ± 19	8,885 ± 265

[1] Data represent the mean ± standard error of the mean of two independent experiments with six replicates each.

TABLE S4[1]

Affinity constants for reference melanocortin ligand binding to the crystallization construct C5[2]

Ligand	pK_i ± S.E.M. (K_i nM)[3]
α-MSH	7.10 ± 0.02 (80.4)
NDP-MSH	9.66 ± 0.03 (0.22)
SHU9119	9.81 ± 0.03 (0.15)
$AgRP_{(83-132)}$	8.53 ± 0.02 (2.94)

[1] Related to Fig. 2B.

[2] Crude cell homogenates were prepared from cells transiently transfected with construct C5 as described in the Materials and Methods section of the Supplemental Materials.

[3] Data were fit by non-linear regression to a one-site sigmoid competition model. K_i values were determined applying the Cheng and Prusoff correction (*54*). Data represent the mean ± standard error of the mean of two independent experiments with six replicates each.

TABLE S5[1]

Potency and efficacy values for reference melanocortin compounds on the relative intracellular cAMP levels measured in live cells transfected with constructs C1 through C5[2]

Construct	α-MSH		SHU9119		$AgRP_{(83-132)}$	
	pEC_{50} ± S.E.M.[3] (EC_{50} nM)	Efficacy[4]	pIC_{50} ± S.E.M.[5] (IC_{50} nM)	Efficacy[4]	pIC_{50} ± S.E.M.[5] (IC_{50} nM)	Efficacy[4]
C1	8.03 ± 0.04 (9.3)	100	7.72 ± 0.03 (19.0)	100	6.89 ± 0.03 (130)	100
C2	7.75 ± 0.02 (17.7)	128	7.95 ± 0.02 (11.3)	86	7.02 ± 0.02 (96)	135
C3	7.82 ± 0.03 (15.1)	148	7.97 ± 0.02 (10.7)	119	6.96 ± 0.01 (110)	172
C4	7.99 ± 0.03 (10.2)	126	7.79 ± 0.02 (16.1)	150	7.07 ± 0.01 (84)	106
C5	NR[6]	NR[6]	NR[6]	NR[6]	NR[6]	NR[6]

[1] Related to Fig. 2C and Fig. S4C, D.

[2] HEK293 cells stably expressing the GScAMP22F cAMP reporter were transfected with 10 µg of plasmid DNA with the sequences of C1 through C5 (Fig. 2A).

[3] Data were fit by non-linear regression to a one-site, four parameters, variable-slope sigmoid stimulus (α-MSH) or inhibition (SHU9119 or $AgRP_{(83-132)}$) model. Data represent the mean ± standard error of the mean of two independent experiments with twelve replicates.

[4] Efficacy values represent the maximum effect in percentage relative to construct C1.

[5] SHU9119 and $AgRP_{(83-132)}$ inhibition profiles were determined in the presence of 30 nM α-MSH; corresponding to an agonist concentration equivalent to EC_{90}.

[6] NR; no response.

TABLE S6[1]

Assessment of coupling of receptor forms C1, C5, and MC4R mutant D122$^{3.25}$A[2] **to Kir7.1**[3] **in response to α-MSH or AgRP$_{(83-132)}$**

Construct	α-MSH pIC$_{50}$ ± S.E.M. (IC$_{50}$ nM)[4]	AgRP$_{(83-132)}$ pEC$_{50}$ ± S.E.M. (EC$_{50}$ pM)[5]
C1	8.67 ± 0.02 (2.12)	9.20 ± 0.06 (637)
C5	8.56 ± 0.01 (2.76)	10.64 ± 0.07 (23)
MC4R D122$^{3.25}$A	NR[6]	NR[6]

[1] Related to Fig. 2E, F.

[2] HEK293 cells were transfected with plasmid DNA with the sequences of constructs C1, C5 (Fig 2A), and mutant receptor D122$^{3.25}$A.

[3] We previously reported the G protein independent coupling of MC4R and Kir7.1 (*13*) as summarized on Fig. 2D.

[4] α-MSH data were fit by non-linear regression to a one-site, four parameter variable-slope sigmoid inhibition model. Data points represent the mean ± standard error of the mean from 3 to 7 different patched cells per compound concentration acquired in two different experimental sessions.

[5] AgRP$_{(83-132)}$ data were fit by non-linear regression to a one-site four parameter variable-slope sigmoid stimulation model. Data points represent the mean ± standard error of the mean from 3 to 7 different patched cells per compound concentration acquired in two different experimental sessions.

[6] NR; no response.

TABLE S7[1]

Effect of different cations on the binding of ^{125}I-NDP-MSH to MC4R[2]

Salt	pEC_{50} ± S.E.M.[3] (EC_{50} μM)	Hill slope
$CaCl_2$	5.43 ± 0.03 (3.74)	2.02 ± 0.27
$ZnSO_4$	5.50 ± 0.07 (3.13)	2.56 ± 0.31
$MgCl_2$	5.23 ± 0.08 (5.96)	1.46 ± 0.39
LiCl	NR[4]	NR[4]
KCl	NR[4]	NR[4]

[1] Related to Fig. 4C.

[2] Crude cell homogenate was prepared from cells stably expressing the wild-type untagged human MC4R as described in the Materials and Methods section of the Supplemental Materials.

[3] Data were fit by non-linear regression to a one-site, variable slope, sigmoid stimulus model. Data represent the mean ± standard error of the mean of two independent experiments with six replicates.

[4] NR; no response.

TABLE S8[1]

Effect of 10 µM $CaCl_2$ on the competition binding profile of SHU9119, NDP-MSH, α-MSH, and $AgRP_{(82-132)}$ to MC4R[2]

Condition	SHU9119 pK_i ± S.E.M. (K_i pM)[3]	NDP-MSH pK_i ± S.E.M. (K_i pM)[3]	α-MSH pK_i ± S.E.M. (K_i nM)[3]	$AgRP_{(83-132)}$ pK_i ± S.E.M. (K_i pM)[3]
Vehicle	10.22 ± 0.04 (60.0)	10.38 ± 0.04 (42.1)	7.19 ± 0.05 (64.2)	9.78 ± 0.07 (167.1)
10 µM $CaCl_2$	10.76 ± 0.04 (17.3)	10.83 ± 0.03 (14.7)	8.77 ± 0.03 (1.71)	10.09 ± 0.04 (82.1)
Fold change	3.47	2.86	37.5	2.04

[1] Related to Fig. 4D.

[2] Crude cell homogenate was prepared from cells transiently transfected with wild-type untagged human MC4R as described in the Materials and Methods section of the Supplemental Materials.

[3] Data were fit by non-linear regression to a one-site sigmoid competition model. K_i values were determined applying the Cheng and Prusoff correction (*54*). Data represent the mean ± standard error of the mean of two independent experiments with six replicates.

TABLE S9[1]

Effect of 100 μM $CaCl_2$ on the binding affinity of α-MSH for MC4R constructs C1 and C5[2]

Condition	MC4R C1 pK_i ± S.E.M. (K_i nM)[3]	MC4R C5 pK_i ± S.E.M. (K_i nM)[3]
Vehicle	7.15 ± 0.04 (110.9)	7.18 ± 0.04 (54.0)
100 μM $CaCl_2$	8.24 ± 0.05 (4.02)	9.18 ± 0.03 (0.55)
Fold change	27.59	98.86

[1] Related to Fig. S4.

[2] Crude cell homogenates were prepared from cells transiently transfected with wild-type tagged human MC4R (C1) or construct C5 incorporating thermostabilizing mutations, N- and C- termini deletions, and PGS fusion (Fig. 2A) as described in the Materials and Methods section of the Supplemental Materials.

[3] Data were fit by non-linear regression to a one-site sigmoid competition model. K_i values were determined by applying the Cheng and Prusoff correction (*54*). Data represent the mean ± standard error of the mean of two independent experiments with six replicates each.

TABLE S10[1]

Effect of 0.5 mM $CaCl_2$ on intracellular cAMP accumulation after α-MSH or Forskolin stimulation of wild type MC4R transfected or untransfected HEK293 cells and receptor - Kir7.1 coupling[2,3]

Condition	α-MSH CRC - LANCE – cAMP accumulation pEC_{50} ± S.E.M. (EC_{50} nM)[4]	Forskolin CRC - LANCE – cAMP accumulation pEC_{50} ± S.E.M. (EC_{50} nM)[4]	MC4R/Kir7.1 coupling pIC_{50} ± S.E.M. (IC_{50} nM)[5]
Ca^{2+} free buffer[6]	6.514 ± 0.06 (309.1)	6.671 ± 0.04 (213.4)	7.31 ± 0.12 (49.0)
0.5 mM $CaCl_2$	9.315 ± 0.07 (0.49)	6.424 ± 0.02 (376.8)	8.17 ± 0.03 (6.76)
Fold change	631	0.57	7.25

[1] Related to Fig. 4E-G.

[2] Untransfected (Forskolin) or transfected (α-MSH) HEK293 cells transfected with constructs C1 (LANCE cAMP accumulation assay) or C1 and Kir7.1(MC4R/Kir7.1 coupling assays) (Fig 2A).

[3] We previously reported the G protein independent coupling of MC4R and Kir7.1 (*13*) as summarized on Fig 2D.

[4] LANCE intracellular cAMP accumulation assay data were fit by non-linear regression to a one-site, four parameter, variable-slope sigmoid model. Data represent the mean ± standard error of the mean of two independent experiments with four replicates.

[5] MC4R/Kir7.1 coupling assay data were fit by non-linear regression to a one-site, three parameter sigmoid inhibition model. Data points represent the mean ± standard error of the mean from 10 to 15 different patched cells per compound concentration acquired in two different experimental sessions.

[6] Ca^{2+} free buffer containing an estimated [Ca^{2+}] ~3 nM consists of 135 mM NaCl, 5 mM KCl, 1 mM EGTA, 5 mM D-glucose, 10 mM HEPES; pH = 7.4 (NaOH) and ~290 mOsmol/kg. Free Ca^{2+} concentration of 0.5 mM was obtained by adding 1.5 mM $CaCl_2$ to this solution.

References and Notes

1. W. Fan, B. A. Boston, R. A. Kesterson, V. J. Hruby, R. D. Cone, Role of melanocortinergic neurons in feeding and the agouti obesity syndrome. *Nature* **385**, 165–168 (1997).

2. D. Huszar, C. A. Lynch, V. Fairchild-Huntress, J. H. Dunmore, Q. Fang, L. R. Berkemeier, W. Gu, R. A. Kesterson, B. A. Boston, R. D. Cone, F. J. Smith, L. A. Campfield, P. Burn, F. Lee, Targeted disruption of the melanocortin-4 receptor results in obesity in mice. *Cell* **88**, 131–141 (1997).

3. E. J. Anderson, I. Çakir, S. J. Carrington, R. D. Cone, M. Ghamari-Langroudi, T. Gillyard, L. E. Gimenez, M. J. Litt, 60 YEARS OF POMC: Regulation of feeding and energy homeostasis by α-MSH. *J. Mol. Endocrinol.* **56**, T157–T174 (2016).

4. M. D. Ericson, C. J. Lensing, K. A. Fleming, K. N. Schlasner, S. R. Doering, C. Haskell-Luevano, Bench-top to clinical therapies: A review of melanocortin ligands from 1954 to 2016. *Biochim. Biophys. Acta Mol. Basis Dis.* **1863** (10 Pt A), 2414–2435 (2017).

5. K. G. Mountjoy, M. T. Mortrud, M. J. Low, R. B. Simerly, R. D. Cone, Localization of the melanocortin-4 receptor (MC4-R) in neuroendocrine and autonomic control circuits in the brain. *Mol. Endocrinol.* **8**, 1298–1308 (1994).

6. J. A. Ballesteros, H. Weinstein, in *Receptor Molecular Biology*, S. C. Sealfon, Ed. (Academic Press, 1995), vol. 25, pp. 366-428.

7. C. Lubrano-Berthelier, B. Dubern, J. M. Lacorte, F. Picard, A. Shapiro, S. Zhang, S. Bertrais, S. Hercberg, A. Basdevant, K. Clement, C. Vaisse, Melanocortin 4 receptor mutations in a large cohort of severely obese adults: Prevalence, functional classification, genotype-phenotype relationship, and lack of association with binge eating. *J. Clin. Endocrinol. Metab.* **91**, 1811–1818 (2006).

8. R. Rong, Y. X. Tao, B. M. Cheung, A. Xu, G. C. Cheung, K. S. Lam, Identification and functional characterization of three novel human melanocortin-4 receptor gene variants in an obese Chinese population. *Clin. Endocrinol. (Oxf.)* **65**, 198–205 (2006).

9. L. A. Lotta, J. Mokrosiński, E. Mendes de Oliveira, C. Li, S. J. Sharp, J. Luan, B. Brouwers, V. Ayinampudi, N. Bowker, N. Kerrison, V. Kaimakis, D. Hoult, I. D. Stewart, E. Wheeler, F. R. Day, J. R. B. Perry, C. Langenberg, N. J. Wareham, I. S. Farooqi, human gain-of-function MC4R variants show signaling bias and protect against obesity. *Cell* **177**, 597–607.e9 (2019).

10. M. M. Ollmann, B. D. Wilson, Y. K. Yang, J. A. Kerns, Y. Chen, I. Gantz, G. S. Barsh, Antagonism of central melanocortin receptors in vitro and in vivo by agouti-related protein. *Science* **278**, 135–138 (1997).

11. T. R. Büch, D. Heling, E. Damm, T. Gudermann, A. Breit, Pertussis toxin-sensitive signaling of melanocortin-4 receptors in hypothalamic GT1-7 cells defines agouti-related protein as a biased agonist. *J. Biol. Chem.* **284**, 26411–26420 (2009).

12. M. Asai, S. Ramachandrappa, M. Joachim, Y. Shen, R. Zhang, N. Nuthalapati, V. Ramanathan, D. E. Strochlic, P. Ferket, K. Linhart, C. Ho, T. V. Novoselova, S. Garg, M. Ridderstråle, C. Marcus, J. N. Hirschhorn, J. M. Keogh, S. O'Rahilly, L. F. Chan, A. J.

Clark, I. S. Farooqi, J. A. Majzoub, Loss of function of the melanocortin 2 receptor accessory protein 2 is associated with mammalian obesity. *Science* **341**, 275–278 (2013).

13. M. Ghamari-Langroudi, G. J. Digby, J. A. Sebag, G. L. Millhauser, R. Palomino, R. Matthews, T. Gillyard, B. L. Panaro, I. R. Tough, H. M. Cox, J. S. Denton, R. D. Cone, G-protein-independent coupling of MC4R to Kir7.1 in hypothalamic neurons. *Nature* **520**, 94–98 (2015).

14. P. Kühnen, K. Clément, S. Wiegand, O. Blankenstein, K. Gottesdiener, L. L. Martini, K. Mai, U. Blume-Peytavi, A. Grüters, H. Krude, Proopiomelanocortin Deficiency Treated with a Melanocortin-4 Receptor Agonist. *N. Engl. J. Med.* **375**, 240–246 (2016).

15. K. Clément, H. Biebermann, I. S. Farooqi, L. Van der Ploeg, B. Wolters, C. Poitou, L. Puder, F. Fiedorek, K. Gottesdiener, G. Kleinau, N. Heyder, P. Scheerer, U. Blume-Peytavi, I. Jahnke, S. Sharma, J. Mokrosinski, S. Wiegand, A. Müller, K. Weiß, K. Mai, J. Spranger, A. Grüters, O. Blankenstein, H. Krude, P. Kühnen, MC4R agonism promotes durable weight loss in patients with leptin receptor deficiency. *Nat. Med.* **24**, 551–555 (2018).

16. K. Y. Chen, R. Muniyappa, B. S. Abel, K. P. Mullins, P. Staker, R. J. Brychta, X. Zhao, M. Ring, T. L. Psota, R. D. Cone, B. L. Panaro, K. M. Gottesdiener, L. H. Van der Ploeg, M. L. Reitman, M. C. Skarulis, RM-493, a melanocortin-4 receptor (MC4R) agonist, increases resting energy expenditure in obese individuals. *J. Clin. Endocrinol. Metab.* **100**, 1639–1645 (2015).

17. J. R. Greenfield, J. W. Miller, J. M. Keogh, E. Henning, J. H. Satterwhite, G. S. Cameron, B. Astruc, J. P. Mayer, S. Brage, T. C. See, D. J. Lomas, S. O'Rahilly, I. S. Farooqi, Modulation of blood pressure by central melanocortinergic pathways. *N. Engl. J. Med.* **360**, 44–52 (2009).

18. R. Krishna, B. Gumbiner, C. Stevens, B. Musser, M. Mallick, S. Suryawanshi, L. Maganti, H. Zhu, T. H. Han, L. Scherer, B. Simpson, D. Cosgrove, K. Gottesdiener, J. Amatruda, B. J. Rolls, J. Blundell, G. A. Bray, K. Fujioka, S. B. Heymsfield, J. A. Wagner, G. A. Herman, Potent and selective agonism of the melanocortin receptor 4 with MK-0493 does not induce weight loss in obese human subjects: Energy intake predicts lack of weight loss efficacy. *Clin. Pharmacol. Ther.* **86**, 659–666 (2009).

19. B. Zarzycka, S. A. Zaidi, B. L. Roth, V. Katritch, Harnessing Ion-Binding Sites for GPCR Pharmacology. *Pharmacol. Rev.* **71**, 571–595 (2019).

20. A. D. White, F. Fang, F. G. Jean-Alphonse, L. J. Clark, H. J. An, H. Liu, Y. Zhao, S. L. Reynolds, S. Lee, K. Xiao, I. Sutkeviciute, J. P. Vilardaga, Ca2+ allostery in PTH-receptor signaling. *Proc. Natl. Acad. Sci. U.S.A.* **116**, 3294–3299 (2019).

21. C. Zhang, Y. Srinivasan, D. H. Arlow, J. J. Fung, D. Palmer, Y. Zheng, H. F. Green, A. Pandey, R. O. Dror, D. E. Shaw, W. I. Weis, S. R. Coughlin, B. K. Kobilka, High-resolution crystal structure of human protease-activated receptor 1. *Nature* **492**, 387–392 (2012).

22. W. Liu, E. Chun, A. A. Thompson, P. Chubukov, F. Xu, V. Katritch, G. W. Han, C. B. Roth, L. H. Heitman, A. P. IJzerman, V. Cherezov, R. C. Stevens, Structural basis for allosteric regulation of GPCRs by sodium ions. *Science* **337**, 232–236 (2012).

23. B. Holst, C. E. Elling, T. W. Schwartz, Metal ion-mediated agonism and agonist enhancement in melanocortin MC1 and MC4 receptors. *J. Biol. Chem.* **277**, 47662–47670 (2002).

24. L. Birnbaumer, M. Rodbell, Adenyl cyclase in fat cells. II. Hormone receptors. *J. Biol. Chem.* **244**, 3477–3482 (1969).

25. Y. Salomon, Melanocortin receptors: Targets for control by extracellular calcium. *Mol. Cell. Endocrinol.* **70**, 139–145 (1990).

26. P. Popov, I. Bizin, M. Gromiha, K. A, D. Frishman, Prediction of disease-associated mutations in the transmembrane regions of proteins with known 3D structure. *eLife* **7**, e34729 (2018).

27. B. Stauch, L. C. Johansson, J. D. McCorvy, N. Patel, G. W. Han, X. P. Huang, C. Gati, A. Batyuk, S. T. Slocum, A. Ishchenko, W. Brehm, T. A. White, N. Michaelian, C. Madsen, L. Zhu, T. D. Grant, J. M. Grandner, A. Shiriaeva, R. H. J. Olsen, A. R. Tribo, S. Yous, R. C. Stevens, U. Weierstall, V. Katritch, B. L. Roth, W. Liu, V. Cherezov, Structural basis of ligand recognition at the human MT1 melatonin receptor. *Nature* **569**, 284–288 (2019).

28. Y. K. Yang, T. M. Fong, C. J. Dickinson, C. Mao, J. Y. Li, M. R. Tota, R. Mosley, L. H. Van Der Ploeg, I. Gantz, Molecular determinants of ligand binding to the human melanocortin-4 receptor. *Biochemistry* **39**, 14900–14911 (2000).

29. Y. Yang, C. M. Harmon, Molecular signatures of human melanocortin receptors for ligand binding and signaling. *Biochim. Biophys. Acta Mol. Basis Dis.* **1863** (10 Pt A), 2436–2447 (2017).

30. Y. X. Tao, Molecular mechanisms of the neural melanocortin receptor dysfunction in severe early onset obesity. *Mol. Cell. Endocrinol.* **239**, 1–14 (2005).

31. Y. Yang, M. Chen, Y. Lai, I. Gantz, K. E. Georgeson, C. M. Harmon, Molecular determinants of human melanocortin-4 receptor responsible for antagonist SHU9119 selective activity. *J. Biol. Chem.* **277**, 20328–20335 (2002).

32. A. J. Venkatakrishnan, X. Deupi, G. Lebon, C. G. Tate, G. F. Schertler, M. M. Babu, Molecular signatures of G-protein-coupled receptors. *Nature* **494**, 185–194 (2013).

33. S. Kopanchuk, S. Veiksina, R. Petrovska, I. Mutule, M. Szardenings, A. Rinken, J. E. Wikberg, Co-operative regulation of ligand binding to melanocortin receptor subtypes: Evidence for interacting binding sites. *Eur. J. Pharmacol.* **512**, 85–95 (2005).

34. M. E. Hadley, B. Anderson, C. B. Heward, T. K. Sawyer, V. J. Hruby, Calcium-dependent prolonged effects on melanophores of [4-norleucine, 7-D-phenylalanine]-alpha-melanotropin. *Science* **213**, 1025–1027 (1981).

35. C. Cao, Q. Tan, C. Xu, L. He, L. Yang, Y. Zhou, Y. Zhou, A. Qiao, M. Lu, C. Yi, G. W. Han, X. Wang, X. Li, H. Yang, Z. Rao, H. Jiang, Y. Zhao, J. Liu, R. C. Stevens, Q. Zhao, X. C. Zhang, B. Wu, Structural basis for signal recognition and transduction by platelet-activating-factor receptor. *Nat. Struct. Mol. Biol.* **25**, 488–495 (2018).

36. G. Fenalti, P. M. Giguere, V. Katritch, X. P. Huang, A. A. Thompson, V. Cherezov, B. L. Roth, R. C. Stevens, Molecular control of δ-opioid receptor signalling. *Nature* **506**, 191–196 (2014).

37. J. L. Miller-Gallacher, R. Nehmé, T. Warne, P. C. Edwards, G. F. Schertler, A. G. Leslie, C. G. Tate, The 2.1 Å resolution structure of cyanopindolol-bound β1-adrenoceptor identifies an intramembrane Na+ ion that stabilises the ligand-free receptor. *PLOS ONE* **9**, e92727 (2014).

38. K. Hirata, K. Yamashita, G. Ueno, Y. Kawano, K. Hasegawa, T. Kumasaka, M. Yamamoto, ZOO: An automatic data-collection system for high-throughput structure analysis in protein microcrystallography. *Acta Crystallogr. D Struct. Biol.* **75**, 138–150 (2019).

39. W. Kabsch, XDS. *Acta Crystallogr. D Biol. Crystallogr.* **66**, 125–132 (2010).

40. A. J. McCoy, R. W. Grosse-Kunstleve, P. D. Adams, M. D. Winn, L. C. Storoni, R. J. Read, *Phaser* crystallographic software. *J. Appl. Crystallogr.* **40**, 658–674 (2007).

41. P. D. Adams, R. W. Grosse-Kunstleve, L. W. Hung, T. R. Ioerger, A. J. McCoy, N. W. Moriarty, R. J. Read, J. C. Sacchettini, N. K. Sauter, T. C. Terwilliger, *PHENIX*: Building new software for automated crystallographic structure determination. *Acta Crystallogr. D Biol. Crystallogr.* **58**, 1948–1954 (2002).

42. B. E. Bricogne G., Brandl M., Flensburg C., Keller P., Paciorek W., Roversi P, Sharff A., Smart O. S., Vonrhein C., Womack T. O., BUSTER version 2.10.2 (Global Phasing, Ltd., 2017); XXXX.

43. P. Emsley, K. Cowtan, Coot: Model-building tools for molecular graphics. *Acta Crystallogr. D Biol. Crystallogr.* **60**, 2126–2132 (2004).

44. J. E. Chrencik, C. B. Roth, M. Terakado, H. Kurata, R. Omi, Y. Kihara, D. Warshaviak, S. Nakade, G. Asmar-Rovira, M. Mileni, H. Mizuno, M. T. Griffith, C. Rodgers, G. W. Han, J. Velasquez, J. Chun, R. C. Stevens, M. A. Hanson, Crystal Structure of Antagonist Bound Human Lysophosphatidic Acid Receptor 1. *Cell* **161**, 1633–1643 (2015).

45. T. Hua, K. Vemuri, M. Pu, L. Qu, G. W. Han, Y. Wu, S. Zhao, W. Shui, S. Li, A. Korde, R. B. Laprairie, E. L. Stahl, J. H. Ho, N. Zvonok, H. Zhou, I. Kufareva, B. Wu, Q. Zhao, M. A. Hanson, L. M. Bohn, A. Makriyannis, R. C. Stevens, Z. J. Liu, Crystal structure of the human cannabinoid receptor CB1. *Cell* **167**, 750–762.e14 (2016).

46. M. A. Hanson, C. B. Roth, E. Jo, M. T. Griffith, F. L. Scott, G. Reinhart, H. Desale, B. Clemons, S. M. Cahalan, S. C. Schuerer, M. G. Sanna, G. W. Han, P. Kuhn, H. Rosen, R. C. Stevens, Crystal structure of a lipid G protein-coupled receptor. *Science* **335**, 851–855 (2012).

47. X. Li, T. Hua, K. Vemuri, J. H. Ho, Y. Wu, L. Wu, P. Popov, O. Benchama, N. Zvonok, K. Locke, L. Qu, G. W. Han, M. R. Iyer, R. Cinar, N. J. Coffey, J. Wang, M. Wu, V. Katritch, S. Zhao, G. Kunos, L. M. Bohn, A. Makriyannis, R. C. Stevens, Z. J. Liu, Crystal Structure of the Human Cannabinoid Receptor CB2. *Cell* **176**, 459–467.e13 (2019).

48. H. Fan, S. Chen, X. Yuan, S. Han, H. Zhang, W. Xia, Y. Xu, Q. Zhao, B. Wu, Structural basis for ligand recognition of the human thromboxane A2 receptor. *Nat. Chem. Biol.* **15**, 27–33 (2019).

49. J. Yin, K. Babaoglu, C. A. Brautigam, L. Clark, Z. Shao, T. H. Scheuermann, C. M. Harrell, A. L. Gotter, A. J. Roecker, C. J. Winrow, J. J. Renger, P. J. Coleman, D. M. Rosenbaum, Structure and ligand-binding mechanism of the human OX1 and OX2 orexin receptors. *Nat. Struct. Mol. Biol.* **23**, 293–299 (2016).

50. P. Egloff, M. Hillenbrand, C. Klenk, A. Batyuk, P. Heine, S. Balada, K. M. Schlinkmann, D. J. Scott, M. Schütz, A. Plückthun, Structure of signaling-competent neurotensin receptor 1 obtained by directed evolution in Escherichia coli. *Proc. Natl. Acad. Sci. U.S.A.* **111**, E655–E662 (2014).

51. N. Robertson, M. Rappas, A. S. Doré, J. Brown, G. Bottegoni, M. Koglin, J. Cansfield, A. Jazayeri, R. M. Cooke, F. H. Marshall, Structure of the complement C5a receptor bound to the extra-helical antagonist NDT9513727. *Nature* **553**, 111–114 (2018).

52. J. Schöppe, J. Ehrenmann, C. Klenk, P. Rucktooa, M. Schütz, A. S. Doré, A. Plückthun, Crystal structures of the human neurokinin 1 receptor in complex with clinically used antagonists. *Nat. Commun.* **10**, 17 (2019).

53. R. Suno, K. T. Kimura, T. Nakane, K. Yamashita, J. Wang, T. Fujiwara, Y. Yamanaka, D. Im, S. Horita, H. Tsujimoto, M. S. Tawaramoto, T. Hirokawa, E. Nango, K. Tono, T. Kameshima, T. Hatsui, Y. Joti, M. Yabashi, K. Shimamoto, M. Yamamoto, D. M. Rosenbaum, S. Iwata, T. Shimamura, T. Kobayashi, Crystal structures of human orexin 2 receptor bound to the subtype-selective antagonist EMPA. *Structure* **26**, 7–19.e5 (2018).

54. Y. Cheng, W. H. Prusoff, Relationship between the inhibition constant (K1) and the concentration of inhibitor which causes 50 per cent inhibition (I50) of an enzymatic reaction. *Biochem. Pharmacol.* **22**, 3099–3108 (1973).